Observation and analyses of Shear Wave Splitting at the Larderello-Travale geothermal field, Italy.

Davide Piccinini and Gilberto Saccorotti

Istituto Nazionale di Geofisica e Vulcanologia

Sezione di Pisa

Via Uguccione della Faggiola, 32 - 56126 Pisa, Italy

Abstract

We measured shear wave splitting (SWS) parameters from a large dataset of local microearthquakes recorded at the Larderello-Travale geothermal field (LTGF; Tuscany, Italy). For that geothermal area, seismic anisotropy is distributed in the upper crust following a complex pattern. Although the overall trend reflects the strike of the normal faults dominating the region, measurements at the southern and central part of the LTGF show large (up to 90°) deviations from the dominant polarization direction. This anomalous pattern suggests that besides the extensive dilatancy anisotropy, the fast wave polarization direction is also likely affected by the presence of over-pressurized geothermal fluids, by local rearrangement of the regional stress, and by the presence of non-vertical cracks. We found large differences in normalised delay times between sparse and clustered seismicity. While the average anisotropy percentage is on the order of 1.7%, a significant amount of our measurements exceeds the 4.5%, reaching values as high as 16%. The highest anisotropy percentages are associated with earthquakes located at the center and at the SE margin of the geothermal area, at depths lower than 5km and in the 5-10km range, respectively. This latter occurrence may be interpreted in terms of cracks filled with fluids which, given the expected pressure and temperature conditions, are likely in supercritical conditions. Shear-wave splitting thus confirm to be a powerful tool for better constraining location and extent of those deep fractured rock portions possibly hosting supercritical fluids, that represent the next frontier of geothermal exploitation due to their enhanced heat capacity.

Introduction

Due to their potential of hosting geothermal fluids, fractured rock volumes constitute an important target of geothermal exploration. Within this context, seismic reflection has been widely adopted for deriving indirect clues about deep and potentially productive targets (e.g., Casini et al., 2010). An increase in fracture density induces a decrease of bulk rock density and seismic velocity (Cameli et al., 2000), which in turn may produce strong impedance contrasts responsible of energetic reflections detectable by surface seismic surveys. The presence of aligned fractures also induces anisotropy in the elastic properties of the propagation medium, thus making the velocity of seismic waves dependent on the source-to-receiver direction. Some recent studies thus investigated the potential of azimuthal variation in the amplitude of reflection data (AVAZ) for individuating potentially-productive fractured horizons at depth (e.g., Aleardi et al., 2014, 2015) .

It is now well-established that earthquake-generated shear waves propagating through isotropic rocks containing stress-aligned cracks behave as if the rocks were anisotropic

(Crampin, 1981; Hudson, 1981). This implies that, disregarding its polarization at the source, a shear wave propagating through a cracked medium splits into two: a fast shear wave, whose polarization is usually parallel to the local strike of crack system (or normal to the direction of the minimum horizontal stress), and a slow one polarized perpendicular to it. Fast shear wave polarization is commonly indicated using the term φ.The time delay (δt) between the fast and slow shear waves is directly related to the number of cracks per unit volume in the medium (crack density), to the aspect ratio of the cracks and to the raypath length (Crampin, 1987; Crampin and Lovell, 1991). Therefore, the interpretation of shear-wave splitting parameters (polarization direction of the fast wave and time delay) is an important diagnostic tool for determining the direction and evaluating the bulk properties of subsurface fractures, with obvious implications for hydrocarbon and geothermal exploration (e.g., Elkibbi et al., 2005; Johnson and Savage, 2012; Lou and Rial, 1997; Palgunadi et al., 2017; Rial et al., 2005; Vlahovic et al., 2003).

In this paper we present unprecedented observations of upper crustal seismic anisotropy derived from analysis of shear wave splitting of local earthquakes at the Larderello-Travale geothermal field, Italy (hereinafter referred to as LTGF). We use data collected by up to 20 stations deployed in the frame of a passive experiment which lasted for 15 months during the years 2012-2013. The collected dataset amounts to 1877 measurements of delay time and fast-wave polarization azimuth, which provide clues about crustal heterogeneity, fracturing and local rearrangement of the crustal stresses. Moreover, we find a high anisotropy percentage located in the SE portion of reservoir, suggesting the likely presence of over-pressurized geothermal fluids at depths.

Geological outline of the study area

Located in the inner Northern Apennines, LTGF is a steam-dominated geothermal field which has been commercially exploited since 1913. Up to about 30 years ago the geothermal resource was exploited from an upper reservoir, hosted within mesozoic limestones at depths of 500-1500 m. At present, the steam is withdrawn from a deeper reservoir located in the paleozoic metamorphic units at depths of about 4000 m (Bertini et al., 2006). Both reservoirs are capped by a low permeability formation associated with the so-called Ligurian units.

The thermal state of the area is characterized by a regional anomaly with heat flow up to 1W/m^2 and thermal gradient on the order of 75-100°C/Km (Baldi et al., 1995). The whole geothermal field extends for about 400 km^2 and has a production of more than 1000 kg/s of superheated steam, with a running capacity of about 700 MW.

A characteristic feature of the geothermal field is the occurrence of seismic reflectors, named the K-horizon and H-horizon (Bertini et al., 2006 and references therein). The K-horizon occurs in the 3-6 km depth range, at the top of Quaternary granites (Batini et al., 1978, 1983). This horizon is characterized by a strong amplitude signal of bright-spot type, suggesting the presence of fluids (magmatic, metamorphic, or a combination of both) hosted within a cracked medium.

The culmination of the K-horizon at a depth of nearly 3000 m is in the SE sector of the study area (see location of station REF6 in Figure 1), where The San Pompeo 2 deep well exploded upon reaching a depth of 2930 m. At that depth, lower bounds on bottom hole pressure and temperature are given by the measurements taken at a depth of 2560 m, i.e. 240 bar and 394°C respectively (Fournier, 1991).

Since supercritical conditions for pure water are reached for temperature and pressure respectively greater than 374°C and 220 bars (e.g., Reinsch et al., 2017), the fluid hosted in the rocks surrounding the K-horizon should be in supercritical conditions even if a saline brine is present.

The current productive layers of the LTGF correspond to the H-horizon, located at the top of pre-Quaternary granites and within the surrounding contact metamorphic aureolas, spanning the 2-4 km depth range. The produced fluid has an overall meteoric isotopic signature and is always superheated steam. From the geophysical point of view the features of the K-horizon are similar to those of the H-horizon, suggesting the presence of a fluid phase permeating the rocks.

The area is seismically active; historical data report a maximum intensity of 7 - 8 Mercalli scale for an earthquake occurred in the Travale area in 1724 (Batini et al., 1985). Recent seismicity is of low intensity, with magnitudes generally lower than 4. Early studies (e.g., Batini et al., 1985) indicate that injection and seismicity rates are positively correlated, while maximum magnitudes generally decrease as the rate of injection increases.

The fault system at the LTGF is dominated by normal faults associated with the latest extensional episode which is lasting since the Pliocene. In particular, a re-examination of field data and seismic reflection lines indicates the presence of three major NW-trending, NE-dipping normal faults (Brogi et al., 2003). The present-day stress field is very heterogeneous, as indicated by the large variability of fault plane solutions which include both normal faults with Apenninic (NW-SE) and anti-Apenninic (NE-SW) directions, and strike-slip mechanisms with the P-axis oriented in NW-SE directions (e.g., Kravanja et al., 2000, and reference therein). Available borehole breakouts from the World Stress Map database (Heidbach, 2016) indicates a maximum horizontal compression direction oriented NW-SE in the central part of the LTGF and almost NS in the Travale area (Fig. 1).

Data and method

During the May 2012 – October 2013 time span, we operated a temporary deployment consisting of up to 20 mobile instruments installed over a 50km x 50km region encompassing the whole geothermal area (Fig. 1). Stations were equipped with a variety of instruments, all recording locally on internal storage devices at a sampling rate of 125 Hz.

The collected dataset amounts to more than 2800 earthquakes, which were obtained after processing the continuous data streams using a STA/LTA procedure. The detected earthquakes were then hand-picked and located using a non-linear, probabilistic procedure (Lomax et al., 2009) acting on travel-times calculated for the 3D tomographic model of Saccorotti et al., (2014).

The obtained hypocenters are generally shallower within the central sector of the area ($z < 5$ km) and are deeper than the top of the *K*-horizon, thus contradicting the hypothesis that such reflector corresponds to the brittle-ductile transition (e.g., Bertani et al., 2005). Moment magnitudes of the recorded dataset range between 1 and 2.9.

Seismicity is diffuse in the whole area, even though some regions are present clusters of seismic events. Due to the spatial distribution of the seismicity and the geometry of the network, azimuthal coverage is rather incomplete, except for those stations located in the central part of the field (eg. LA05).

3

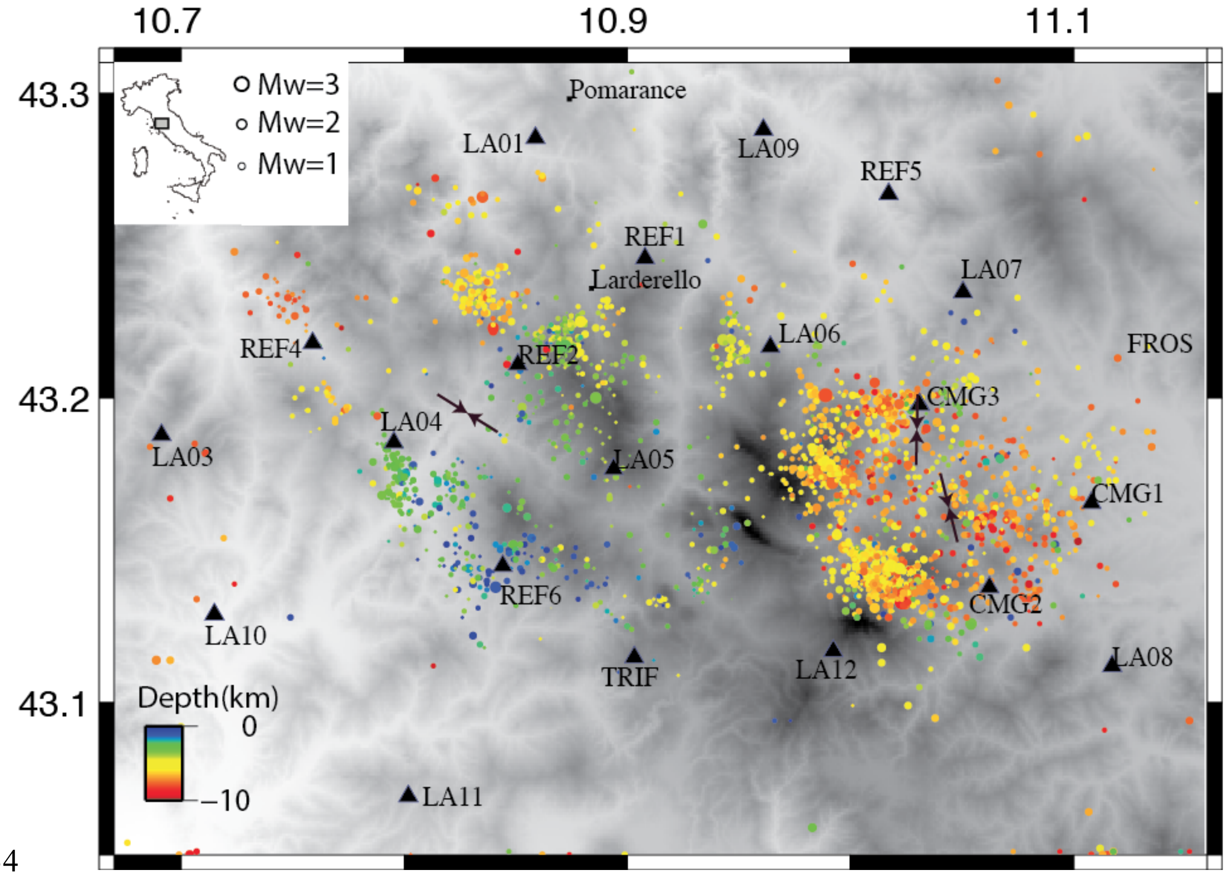

Fig. 1 - Map of seismicity recorded during the GAPSS experiment. epicenters are represented by dots, whose size is proportional to magnitude and color represents depth according to the colorbar at the bottom left. Black triangles represent seismic stations used in this study. Black arrows indicate the direction of maximum horizontal stress available from WSM database. The inset at the top left shows location of the study area with respect to Italy.

We processed the recorded dataset using the code ANISOMAT+ (Piccinini et al. 2013) to estimate the anisotropic parameters, φ and δt. The code is based on the cross-correlation (CC) method (Bowman & Ando 1987) assuming that the S-fast and S-slow horizontal components have similar waveforms. The two horizontal seismograms (the NS and EW components) are rotated in the horizontal plane by 1° azimuthal increment from 0° to 180°. For each trial direction, we evaluate the CC function between the two horizontal seismograms over a given time window. The rotation azimuth at which the maximum of the CC function attains its largest value represents the fast S-wave polarization direction φ and the corresponding time lag is the delay time δt between the S- fast and slow components. For a complete description of the code, the reader is referred to Piccinini et al. (2013).

In order to obtain reliable estimates of the splitting parameters, we selected only those waveforms that satisfy the following criteria:

i) Seismic rays having a geometrical incidence angle $i_c \leq 45°$;

ii) *S*-to-*P* amplitude ratio (calculated as the amplitude of a window starting at the *S*-wave onset divided by the amplitude of a time window containing the *P* wave) > 4;

iii) The Horizontal-to-Vertical (H/V) ratio for the time window containing the S-wave arrival greater than 1;

4

The first restriction guarantees that the S waves do not interact with any free surface or horizontal interface or cracks, ensuring that particle motion was not contaminated from S to P converted phases (Booth & Crampin 1985), free surface effects (Nuttli 1961) and phase changes at crustal discontinuities (Liu & Crampin 1990);

The two latter restrictions aim at rejecting data with possible contamination by the *P*-wave coda (high *S*-to-*P* ratio), and to use only waveforms with small *S*-wave amplitude on the vertical component (high H/V ratio).

To improve the signal-to-noise ratio, all waveforms have been bandpass filtered over the 1–15 Hz frequency band using a Butterworth, fourth-order two-pass filter.

For CC calculations, we used a ~0.3s-long time window starting 0.1 s before the estimated *S*-wave arrival time. To guarantee consistency of results, we consider only those measurements showing a CC coefficient larger than or equal to 0.75. The final shear wave splitting measurements consists of 1877 event-station pair.

SWS Results

Our measurements of φ and δt exhibit significant scattering. Figure 2 summarizes SWS data at all the stations: individual measurements are represented by a bar which is oriented according to φ and whose length is proportional to δt. We excluded from any further analysis data from stations LA09 and LA03 because they worked for a very limited time span. Null measurements are indicated by a circle; station-averaged directions are indicated by a green bar at the center of each plot. The great circle indicates an angle of incidence of 45°. We define as Null those measurements whose δt is equal to zero or, more formally, smaller than the sampling rate (i.e. 0.008 s). Null measurements occur if the waves propagate through an isotropic volume, or if the polarization at the source coincides with the fast or slow direction.

5

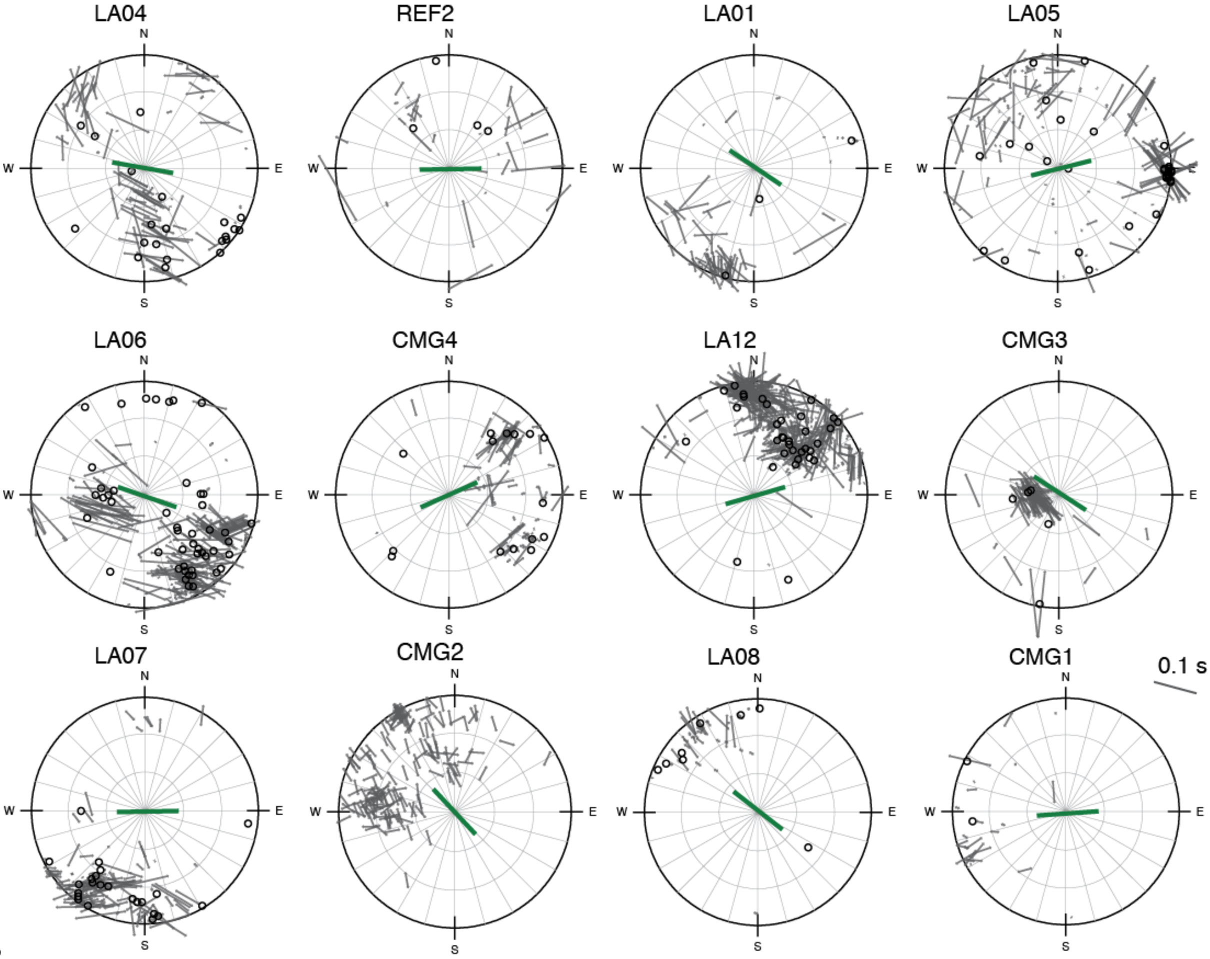

Fig. 2 - Equal-area, lower-hemisphere projection plots of phi measurements for 12 stations in the LTGF area. The plot radius corresponds to an incidence angle of 45°; circles refer to null measurements. The length of individual line segments is proportional to the corresponding δt. The green line segments at the center of each polar diagram represent the average fast direction.

Except for a few stations (e.g. LA04, LA06, LA08, CMG2), the distribution pattern at individual sites is complex, showing the coexistence of different polarizations azimuth. It is worth noting that, in case of tightly-clustered hypocenters, SWS data are mutually consistent, as for instance at station CMG3 whose polarization azimuths are consistently oriented NW-SE.

Analyzing LA04 we note two sets of anisotropy directions: the rays approaching the station from south and from northeast exhibit an average polarization trend oriented NW-SE, while rays approaching from northwest show an almost orthogonal polarization direction. A similar behaviour is observed at station LA06: rays approaching from W and SW show a marked NW-SE anisotropy direction while the anisotropy directions for sources in the SE quadrant are more scattered, exhibiting both NW-SE and NE-SW trends.

Station CMG2 is characterised by a more homogeneous trend oriented NW-SE, but it also shows the coexistence of orthogonal anisotropy directions. Note that CMG2 is located to the SE of the seismicity cluster affecting the Travale area, which is particularly active for which concerns both seismicity rate and production of geothermal energy. Similar considerations hold for site LA12 (SW of the Travale area) which show a very complex and heterogeneous

 6

pattern of anisotropy directions.

Figure 3 illustrates the spatial distribution of the polarisation azimuths and normalized delay times in map view.

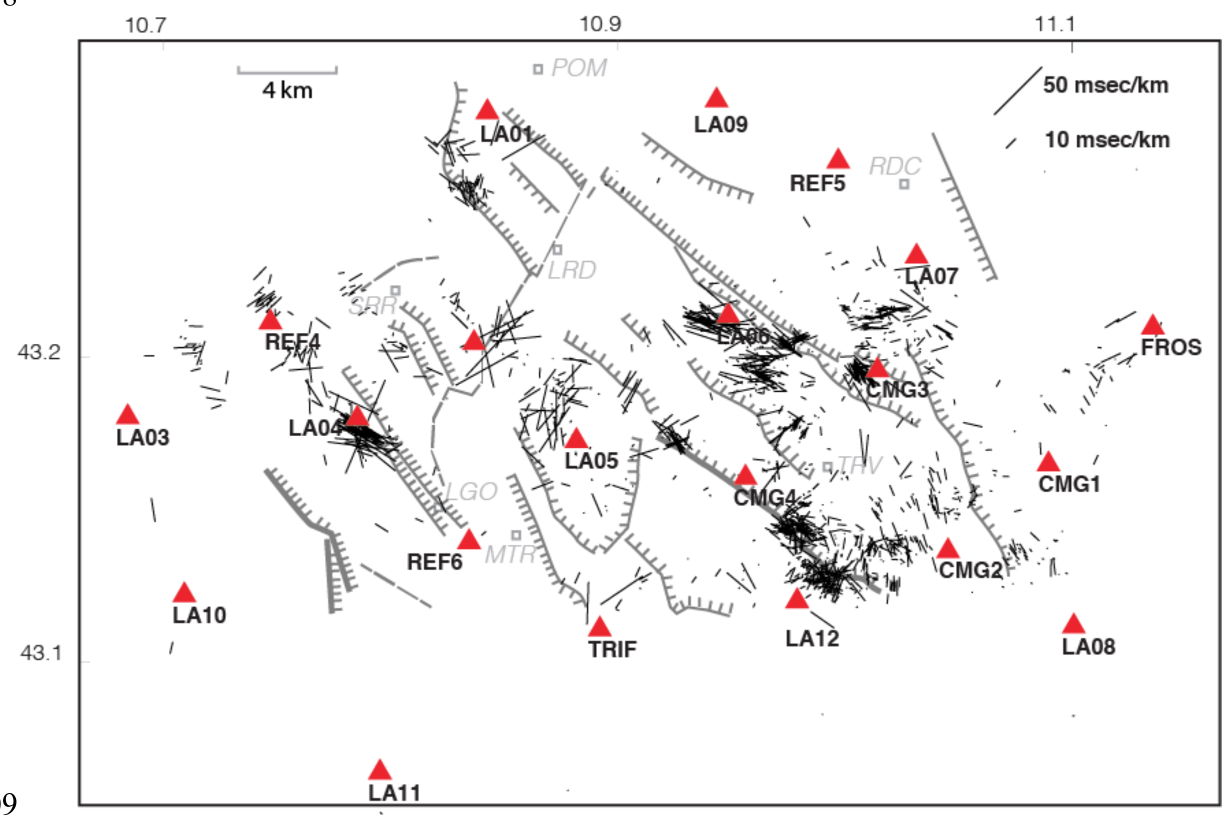

Fig. 3 - Map of polarisation angle φ and normalized δt for the complete dataset. Fault traces in dark gray are taken from Bellani et al. (2004). Black line segments represents polarization direction and magnitude of delay time for each event and are located at the midpoint between the source and the receiver. Red triangles represent seismic station location. In light gray are reported places mentioned in the text: (POM=Pomarance, RDC=Radicondoli, SRR=Serrazzano, LRD=Larderello, TRV=Travale, LGO=Lago Boracifero, MTR=Monterotondo)

The largest normalized δt values are related to the seismicity clusters located at the border of the main productive areas (i.e. Lago, Larderello, Travale). In general, clusters with the largest normalized δt also show an average polarisation direction which is parallel to the local fault pattern, and in particular for the central and western part of the LTGF (see Fig. 3) .

Figure 4 (top left corner) shows the rose diagrams summarizing all the SWS observations. Non-null polarization azimuth distribution (in green) show at least three peaks. The two largest ones are oriented WNW-ESE and NW-SE, which are both consistent with the overall direction of the local fault system. The third peak is barely recognizable and it is oriented along the NE-SW direction. The 467 null measurements (in red) remark the averaged direction of the fault system.

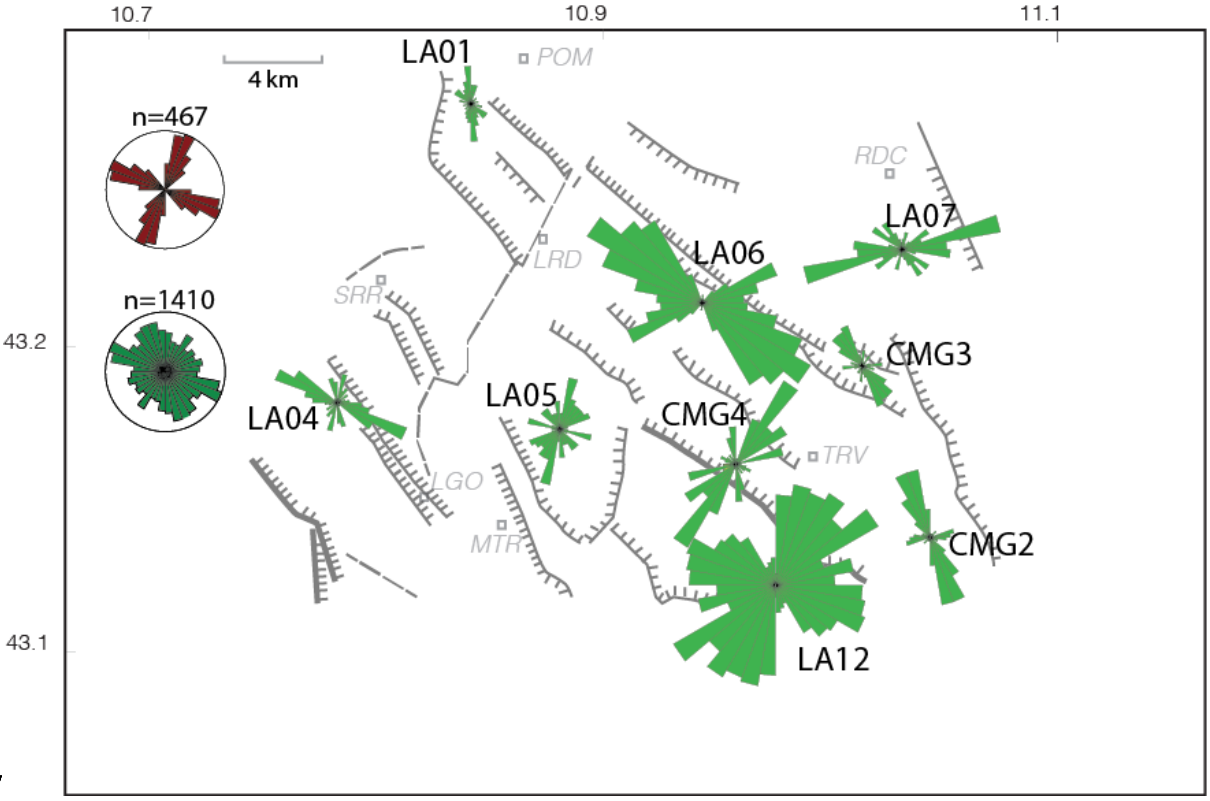

Fig. 4 - Average direction for station with more than 50 valid (cc > 0.75) measures of shear wave splitting. In light green the cumulative rose diagram. In the top left corner we show the cumulative rose diagram for 1410 shear wave splitting measures, and 467 nulls. Size of the rose diagrams are proportional to the total number of measures.

In order to provide a statistical analysis of the obtained results, we applied the Von Mises method to calculate the resultant length *R* and the mean fast direction φ with corresponding standard deviation σ (Table 1; Davis 1986; Mardia & Jupp 2000; Cochran *et al*. 2003). As an example, station LA12 present two broad peaks, one oriented NE-SW and the other oriented WNW-ESE: *R* value for this station is close to 0.6, indicating a largely scattered dataset.

Figure 4 also shows the rose-diagrams of polarisation direction for those stations with more than 50 valid SWS measurements. In general, most stations show a bimodal, often almost orthogonal, distribution. This characteristic could be related to a local rearrangement of fracture field due to the existence of over-pressurized fluids or to the presence of non vertical cracks. These hypotheses will be discussed in detail later.

Due to the bimodal character of the distributions of polarisation directions, the representation of the mean direction can be misleading, notwithstanding the high value of *R*. For this reason, the map does not report the average direction of polarization azimuths.

In order to estimate and quantify the spatial distribution of crack density, we calculate for each event the percentage of anisotropy in terms of the velocity difference between the fast and slow shear waves (Crampin, 1989):

$$S_{anis\%} = 100*(V_{fast} * V_{min})/V_{fast}$$

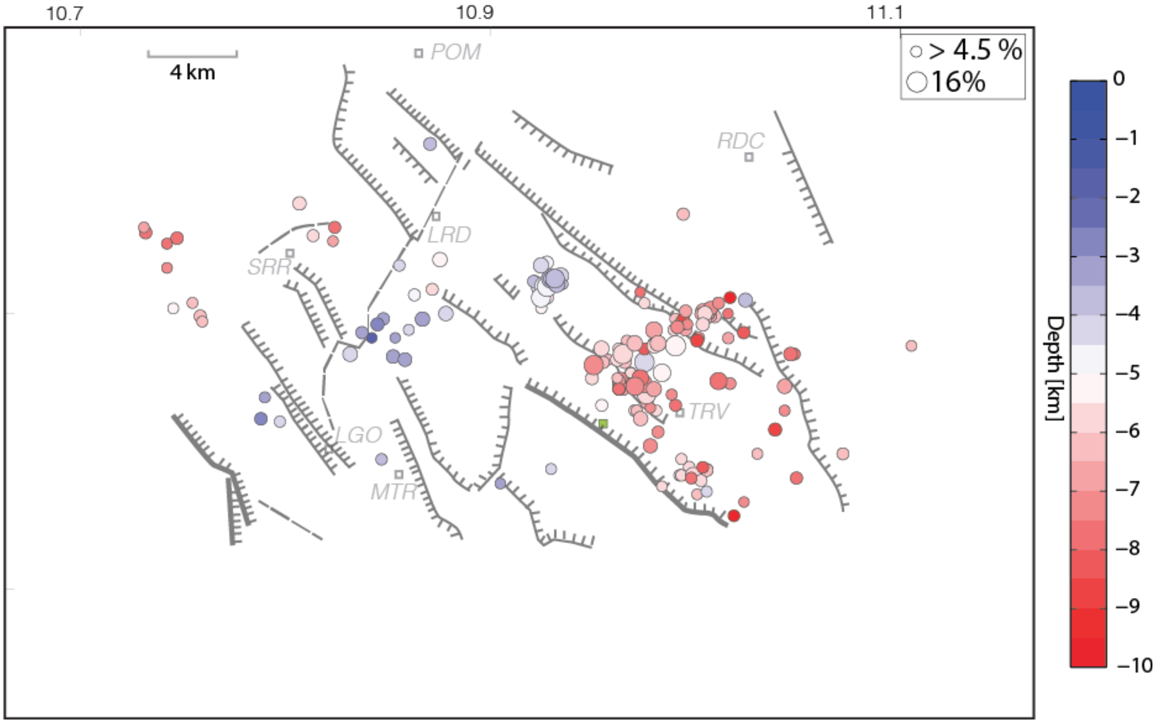

Fig. 5 - Epicenters of earthquakes showing anisotropy percentage larger than 4.5%. Depth is color coded.

For a mean delay time of 51ms (calculated for the whole catalogue), $S_{anis\%}$ is on the order of 1.7%, while for the maximum observed delay of 192ms $S_{anis\%}$ is 16.7%. In order to identify the distribution of the anisotropy percentage and locate the volumes with high crack density, we plot the hypocenters of those earthquakes showing a $S_{anis\%}$ value greater than 4.5%, which represents the lower limit inferred for competent rocks (Crampin, 1994; Fig. 5).

The spatial distribution of percentage anisotropy evidences two different conditions. In the central part of LTGF a small and tight cluster of large $S_{anis\%}$ is associated with a shallow ($z < 5$ km) group of earthquakes. On the other hand, in the Travale area (SE sector of the LTGF) a large number of deep events ($z > 5$ km) show large anisotropy percentage, suggesting the presence of a deep rock volume with large crack density. No clear correlation between earthquakes depth and anisotropy percentage emerges from our results.

We further focused our attention on a small portion of ~10 km^2 located few km north of Travale, in an area characterized by large anisotropy percentage and by the presence of a complicated pattern NW-SE striking, NE dipping branches of normal faults. Figure 6 (upper panel) shows anisotropy measurements at stations CMG3 and LA06, both situated close to one of the fault trace outcropping in the area. The overall fast wave direction reflects the strike of the fault system, except for a small group of earthquakes observed at LA06 and located close to CMG3. For these events, polarization direction are almost perpendicular to the fault strike.

9

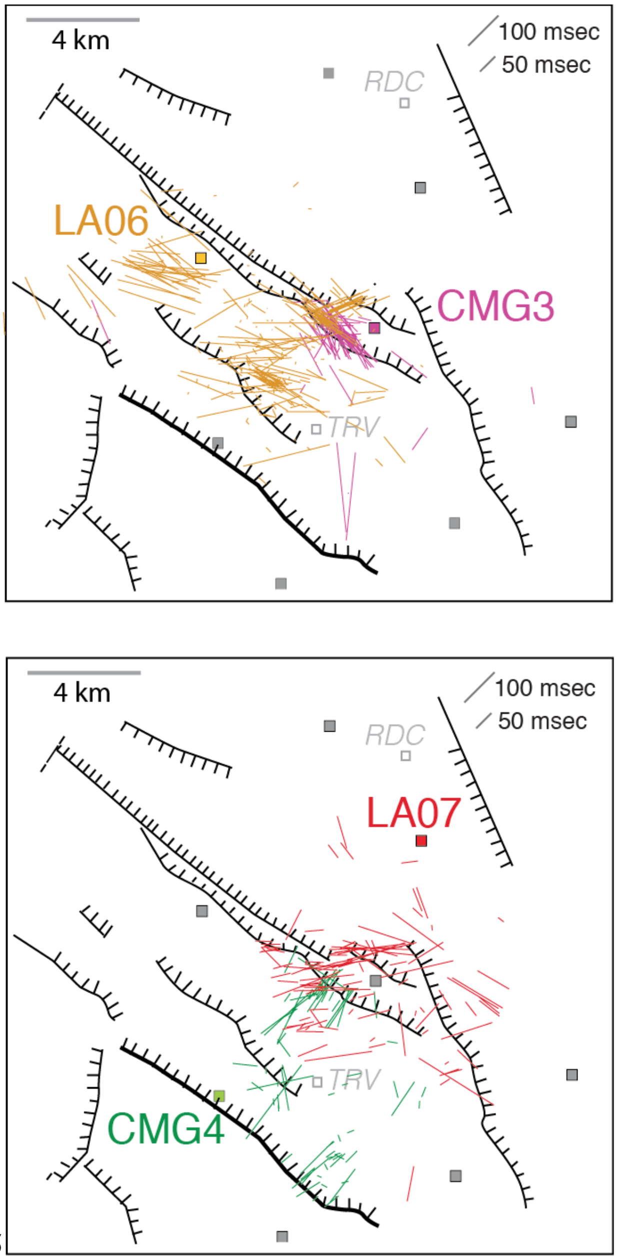

Fig. 6 - SWS observation for Travale area. Line segments length are proportional to the δt. Color of the line segment is relative to the station

Figure 6 (bottom panel) reports SWS observations at CMG4 and LA07, both located along-dip of the same fault system. Both stations show SWS fast direction severely misoriented with respect to the fault strike, with an average direction almost orthogonal to the general fault direction. Overall, the data shown in Figure 6 clearly indicate that sources spanning the same focal volume exhibit different anisotropic behaviours, depending on the back-azimuth and epicentral distance.

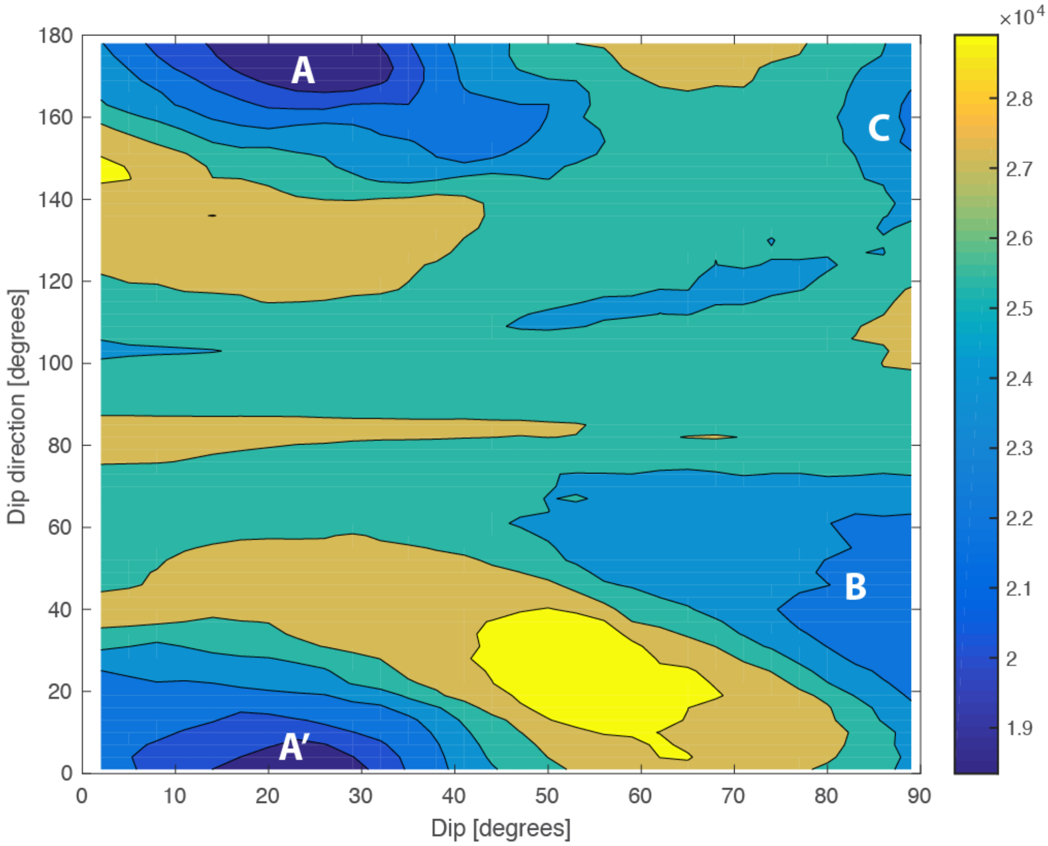

Assuming that the seismic anisotropy is mainly induced by open cracks, microcracks and preferentially-oriented pore spaces, and further assuming that all the fractures along a given raypath have the same orientation and are approximately uniformly distributed, we inverted the measurements illustrated in Figure 6 for dip and dip direction of a fractures set (e.g., Rial et al., 2005). We conducted a grid search over dip direction and dip angles; at each trial angular value, the polarisation directions at the recording sites are compared, in a least-square sense, with those predicted by the corresponding stiffness matrix. The results are illustrated in Figure 7, where the prediction error is mapped against the two angles defining the spatial setting of the fracture field. There are three main sets of minima: the first, corresponds to sub-horizontal fractures (dip ~20°), striking EW +/- 20° (see labels A and A' in Fig. 7). The second minimum (labeled B) corresponds to sub-vertical fractures whose dip direction span the 40°-60° range (i.e., strike between 130°-150°), which is compatible with the Apenninic direction and the orientation of the principal faults of the area, as shown in Figure 6. The third minimum (label C) is representative of sub-vertical fractures striking between 60°- 80°, consistently with the NE-trending, normal- to strike-slip steeply-dipping faults reported by Brogi et al., (2003). While solutions B and C can be directly interpreted in light of well-identified fault systems, different competing hypotheses can be invoked for explaining the minimum-misfit solutions [A, A']

A first, possible explanation relies on the presence of reflective horizons in correspondence of, or above the K-horizon. Such reflectors have been interpreted in terms of shear zones associated with the coalescence at depth of the basal portions of listric faults (e.g., Fig. 4 in Brogi et al., 2003).

A second, possible explanation relies on the sub-horizontal foliation pattern of the micaschist complex locally overlying the granitic intrusions of both Pliocenic and Quaternary ages.

 11

Within the particular crustal volume here discussed, such metamorphic complex is expected at depths between 3km and 5km, and it includes the H-horizon (see Fig. 4 in Bertini et al., 2006).

Discussion and Conclusions

Results from SWS analysis at the LTGF indicate that both the polarization direction of the fast shear wave and the delay time between the two shear waves are distributed according to a complex spatial pattern. As a general consideration, SWS observations related to diffuse seismicity exhibit small δt and scattered polarization directions, independently from the local arrangement of the stress field. Conversely, measurements associated with seismic clusters show the largest delay times, and polarization azimuths which are in good agreement with the average trend of the regional normal faults, and consistent with $S_{H}max$ data from borehole breakouts. In addition, SWS measurements for individual clusters are mutually consistent, thus indicating the reliability of our results.

We individuated two regions characterised by large (up to 16%) anisotropy percentage $S_{anis\%}$. The first one is associated with a cluster of shallow (z < 5 km) seismicity located at the center of the geothermal area. The second one, located at the SE margin of LTGF beneath the Travale area, is associated with larger hypocentral depths (5km<z<10km; Fig. 5). Similar large anisotropy percentage (up to 18%) were also reported by Kaneshima (1988) for a SWS study on Takinoue geothermal area in northern Honshu, Japan. Such large anisotropy percentage imply that the rock is essentially fragmented and in an unstable state. However, exceptions to this scenario are found in the very near surface where confining pressures are small, and in deeper over-pressurized hydraulic compartments (Powley, 1990) where the pore fluids may not easily disperse (Crampin, 1993). Keeping in mind these two possibilities, in Figure 8 we present a general sketch which summarizes a conceptual model for the distribution of highly-anisotropic volumes at the LTGF. Volumes with large $S_{anis\%}$ at shallow depths (*SHAP*) could be related to the low confining pressure at near-surface conditions, which would promote cracks opening. These volumes are mainly located in the central part of the LTGF and could be related to the shallow reservoir. Conversely, the deep high-anisotropy regions (DHAP) encountered at the SE margin of LTGF could be related to high pore pressure and/or fluid-filled cracks. For the depth range spanned by the DHAP, both pressure and temperature conditions indicate that fluids hosted in the cracked volume are in super-critical state. This hypothesis is in agreement with the results presented by Piana Agostinetti *et al.* (2017), who interpreted a sharp reduction in teleseismic P-wave anisotropy throughout the 5-7km depth range with the presence of fluids in supercritical conditions.

12

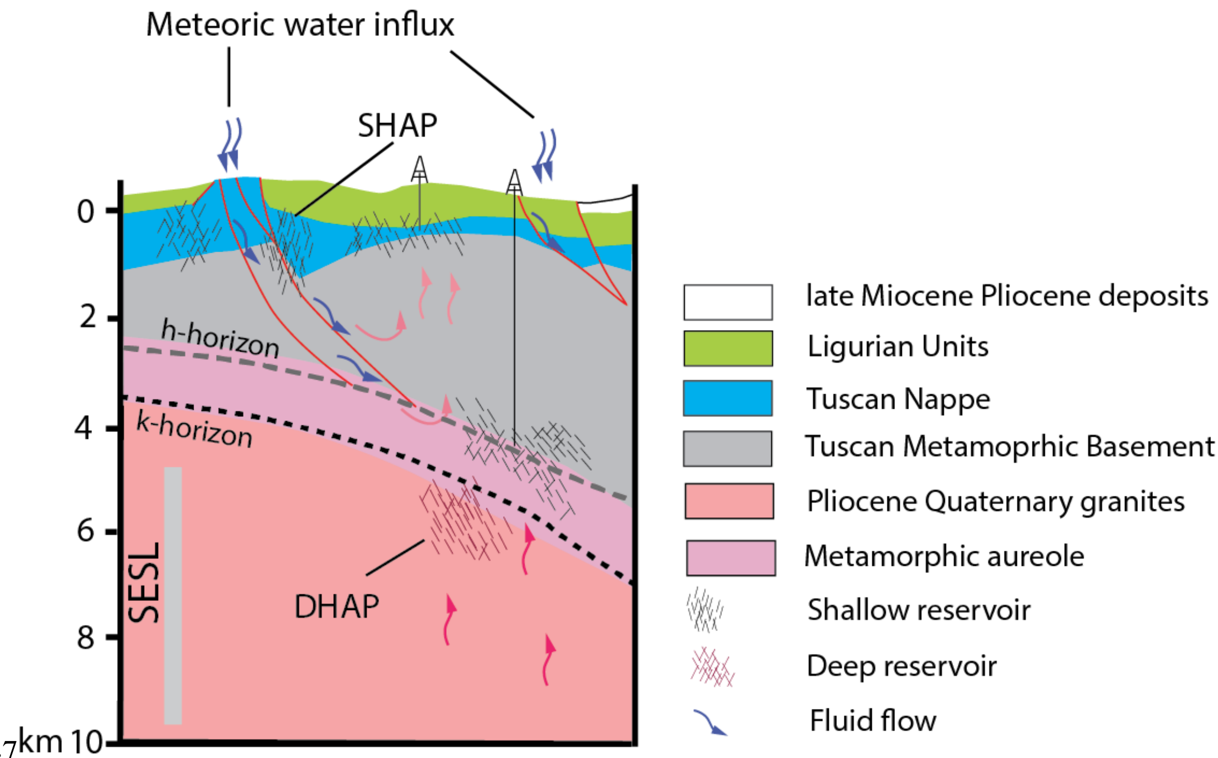

Fig. 8 - Sketch of a conceptual model of LGTF, summarizing the distribution of seismic anisotropy. SHAP=Shallow High Anisotropy Percentage; DHAP Deep High Anisotropy Percentage; SESL: South-Eastern Seismogenic Layer;

Several stations exhibit the coexistence of orthogonal SWS directions for sources spanning small ranges of back-azimuth/distances. This affects particularly those earthquakes/station pairs located in proximity of faults in the Travale area (Fig. 6). Referring to the inversion results illustrated in Figure 7, there are distinct, non-vertical set of fractures along the ray-path which can explain the gross features of our observations. Alternatively, the orthogonal polarization directions can be interpreted in terms of 90° flips in shear-wave polarizations due to the combined presence of fluid-filled, heavily-fractured rocks at critically high pore-fluid pressures (e.g. Crampin, 1997).

In conclusion, the complex patterns revealed by our shear-wave polarisation data demonstrate that regional stress and fault structures cannot entirely explain the upper crustal anisotropy observed at the LTGF. Rather, the distribution of SWS parameters most likely reflects the combined influence of tectonic structures, stress field, and the abundant presence of over-pressurized fluids which locally may reach supercritical conditions. This latter information is of particular relevance, since supercritical fluids have an heat capacity which is much higher than that of subcritical ones, making the former resources the frontier for the next generation of geothermal exploitation programs.

Acknowledgments:

The GAPSS experiment was supported through internal INGV funding; we thanks Claudio Chiarabba, Milena Moretti and the Mobile Seismic Network Team for providing most of the stations used for this study. Data are currently embargoed. Thoughtful discussion with colleagues Lucia Margheriti and Francesco Mazzarini greatly helped to interpret the results.

 13

Careful revision from an anonymous reviewer greatly helped in improving the quality of the manuscript.

Table 1

Sta	**n**	$\varphi(°)$	**R**	σ **(°)**
CMG1	23	86	0.8160	17.3
CMG2	**83**	**137**	**0.8000**	**18.1**
CMG3	**65**	**123**	**0.7413**	**20.6**
CMG4	**83**	**66**	**0.6773**	**23.0**
LA01	**59**	**124**	**0.5370**	**27.5**
LA03	25	70	0.9043	12.5
LA04	**79**	**100**	**0.7131**	**21.7**
LA05	**98**	**76**	**0.5887**	**25.9**
LA06	**219**	**109**	**0.8551**	**15.4**
LA07	**123**	**89**	**0.7902**	**18.5**
LA08	38	128	0.9123	12.0
LA09	16	107	0.8163	17.3
LA12	**340**	**74**	**0.6914**	**22.5**
REF2	28	89	0.5751	26.4

Table 1 - *Station name, number of measurements, mean, length of resultant vector and standard deviation of fast direction for the whole dataset. In boldface stations with more than 50 measurements, also shown in Figure 4.*

References

Aleardi, M., and A. Mazzotti, 2014. A feasibility study on the expected seismic AVA signatures of deep fractured geothermal reservoirs in an intrusive basement. J. Geophys. Eng. doi:10.1088/1742-2132/11/6/065008

Aleardi, M., A. Mazzotti, A. Tognarelli, S. Ciuffi and M. Casini, 2015. Seismic and well log characterization of fractures for geothermal exploration in hard rocks. *Geophys. J. Int.* 203, 270–283. doi: 10.1093/gji/ggv286

Baldi P., S. Bellani, A. Ceccarelli, A. Fiordelisi, P. Squarci and L. Taffi, 1995. “Geothermal anomalies and structural features of southern Tuscany“ Proceedings of the World Geothermal Congress, Florence, Italy,18-31 May 1995, pp 693-696

Batini, F., Burgassi, P.D., Cameli, GM., Nicolich, R. and Squarci. P., 1978. Contribution to the study of the deep lithospheric profiles: Deep reflecting horizons in Larderello-Travale Geothermal field. Mem. Sot. Geol. Ital., 19: 477-484.

Batini, F., Bertini, G., Gianelli, G., Pandeli, E. and Puxeddu, M., 1983. Deep structure of the Larderello field: contribution from recent geophysical and geological data. Soc. Geol. Ital. Mem., 25, 219–235

Batini, F., Console, R., Luongo, G., 1985. Seismological study of the Larderello-Travale geothermal area. Geothermics 14, 255

Bellani S, Brogi A, Lazzarotto A, Liotta D, Ranalli G. (2004) Heat flow, deep temperatures and extensional structures in the Larderello Geothermal Field (Italy): constraints on geothermal fluid flow. J Volcanol Geotherm Res 132:15–29

Bertani, R.: World Geothermal power generation in the period 2001-2005, 2005a, Geothermics, 34, 651-690.

Bertini, G., Casini, M., Gianelli, G. and Pandeli, E. (2006), Geological structure of a long-living geothermal system, Larderello, Italy. Terra Nova, 18: 163–169. doi:10.1111/j.1365-3121.2006.00676.x

Booth, D. C., and Crampin, S., 1985, Shear-wave polarizations on a curved wavefront at an isotropic free-surface: Geophys. J. Roy. Astr. Soc., 83, 31-45

Bowman, J. R. and Ando, M., 1987, Shear-wave splitting in the upper-mantle wedge above the Tonga subduction zone. Geophysical Journal of the Royal Astronomical Society, 88: 25–41. doi:10.1111/j.1365-246X.1987.tb01367.x

Brogi A., Lazzarotto A., Lotta D. Ranalli G., 2003 Extensional shear zones as imaged by reflection seismic lines: the Larderello geothermal field(central Italy) Tectonophysics 363,127-139.

Cameli, G.M., Ceccarelli, A., Dini, I., Mazzotti, A., 2000. Contribution of the seismic reflection method to the location of deep fractured levels in the geothermal fields of southern Tuscany (Central Italy). In: *Proceedings of the 2000 World Geothermal Congress*, Kyushu and Tohoku, Japan, May–June 2000, pp. 1025–1029.

Casini, M., Ciuffi, S., Fiordelisi, A., Mazzotti, A. & Stucchi, E., 2010. Results of a 3-D seismic survey at the Travale (Italy) test site, *Geothermics*, 39(1), 4–12.

Cochran E.S., Vidale J.E. and Li Y.-G. ,2003. Near-fault anisotropy following the Hector Mine earthquake, *J. Geophys. Res*. 108, 9, 2436, doi:10.1029/2002JB002352

Crampin, S., 1981. A review of wave motion in anisotropic and cracked elastic media. Wave Motion 3, 343–391.

Crampin, S., 1987. Geological and industrial implications of extensive-dilatancy anisotropy, Nature, 328, 491-496.

Crampin, S., 1989. Suggestions for a consistent terminology for seismic anisotropy, Geophys. Prospect., 37, 753 – 770.

 15

Crampin, S. & Lovell. J.H., 1991. A decade of shear-wave splitting in the Earth's crust: what does it mean? what use can we make of it? and what should we do next? in Proc. 4th Int. Workshop on Seismic Anisotropy, Edinburgh, 1990, eds. J.H. Lovell & S. Crampin, Geophys. J. Int., 107, 387-407.

Crampin, S., & Leary, P. C., 1993. Limits to Crack Density: The State of Fractures In Crustal Rocks. Society of Exploration Geophysicists.

Crampin, S., 1994. The fracture criticality of crustal rocks. Geophysical Journal International, 118: 428–438. doi:10.1111/j.1365-246X.1994.tb03974.x

Crampin, S. and Zatsepin, S. V. (1997), Modelling the compliance of crustal rock—II. Response to temporal changes before earthquakes. Geophysical Journal International, 129: 495–506. doi:10.1111/j.1365-246X.1997.tb04489.x

Davis J.C. 1986 Statistics and Data Analysis in Geology John Wiley, 646

Fournier, R. O. The transition from hydrostatic to greater than hydrostatic fluid pressure in presently active continental hydrothermal systems in crystalline rock. Geophys. Res. Lett.18, 955–958 (1991).

Elkibbi, M., M. Yang, J.A. Rial, Crack-induced anisotropy models in the geysers geothermal field. Geophys. J. Int., 162 (2005), pp. 1036-1048, 10.1111/j.1365-246X.2005.02697.x

Johnson J.H., Savage, M.K. (2012). Tracking volcanic and geothermal activity with shear wave splitting tomography. Journal of Volcanology and Geothermal Research, 223-224, 1-10.

Heidbach, O., Rajabi, M., Reiter, K., Ziegler, M., WSM Team (2016): World Stress Map Database Release 2016. GFZ Data Services. http://doi.org/10.5880/WSM.2016.001

Hudson, J.A., 1981. Wave speeds and attenuation of elastic waves in material containing cracks. Geophys. J. R.Astr. Soc. 64, 133–150.

Kaneshima, S., Ito, H. & Sugihara, M., (1988). Shear-wave splitting observed above small earthquakes in a geothermal area of Japan, Geophys. J. R. astr SOC., 94, 399-411.

Kravanja, S., Batini, F., Fiordelisi, A. et al. (2000) Full Moment Tensor Retrieval from Waveform Inversion in the Larderello Geothermal Area; Pure appl. geophys. 157: 1379. https://doi.org/10.1007/PL00001124

Liu, E. & Crampin, S., 1990. Effects of the internal shear wave window: comparison with anisotropy induced splitting, J. geophys. Res., 95, 11275-11281

Lomax, A., A. Michelini, A. Curtis, 2009. Earthquake Location, Direct, Global-Search Methods, in Complexity In Encyclopedia of Complexity and System Science, Part 5, Springer, New York, pp. 2449-2473, doi:10.1007/978-0-387-30440-3.

Lou, M., Rial, J.A., (1997). Characterization of geothermal reservoir crack patterns using shear-wave splitting. Geophysics, 62, 487-495.

Mardia K.V and Jupp P.E. (2000) Directional Statistics, John Wiley 429

Nuttli, O. (1961). The effect of the Earth's surface on the S-wave particle motion, Bull. Seism. Soc. Am. 51,237-246.

Palgunadi, K. H., A. D. Nugraha, R. Sule and T. Meidiana. (2017) Steam and Brine Zone Prediction around Geothermal Reservoir Derived from Delay Time Seismic Tomography and Anisotropy Case Study: “PR” Geothermal Field.

Piana Agostinetti N., Licciardi A., Piccinini D., Mazzarini F., Musumeci G., Saccorotti G., and C. Chiarabba. (2017) Discovering geothermal supercritical fluids: a new frontier for seismic exploration. Scientific Reports 7, doi:10.1038/s41598-017-15118-w

Piccinini, D., M. Pastori and L. Margheriti (2013), ANISOMAT+: An automatic tool to retrieve seismic anisotropy from local earthquakes. Computers & Geosciences, http://dx.doi.org/10.1016/j.cageo.2013.01.012i.

Powley, D.E., 1990. Pressures and hydrogeology in petroleum basins, Earth Sci. Rev., 29, 215-226.

Reinsch, T., P. Dobson, H. Asanuma, E. Huenges, F.Poletto and B. Sanjuan, 2017. Utilizing supercritical geothermal systems: a review of past ventures and ongoing research activities. *Geotherm Energy* 5:16 DOI 10.1186/s40517-017-0075-y

Rial JA, Elkibbi M, Yang M., 2005. Shear-wave splitting as a tool for the characterization of geothermal fractured reservoirs: Lessons learned. Geothermics. 34: 365-385. DOI: 10.1016/j.geothermics.2005.03.001

Vlahovic G, Elkibbi M, Rial JA., 2003. Shear-wave splitting and reservoir crack characterization: The Coso geothermal field Journal of Volcanology and Geothermal Research. 120: 123-140. DOI: 10.1016/S0377-0273(02)00368-2

 17